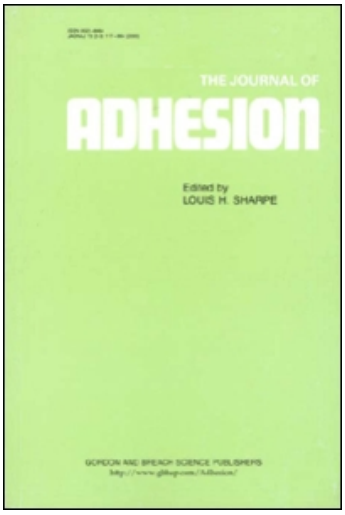

The Journal of Adhesion
Publication details, including instructions for authors and subscription information:
http://www.informaworld.com/smpp/title~content=t713453635

Analytical and Numerical Calculation of the Energy Release Rate for the Microbond-Test

T. Schüller[a]; W. Beckert[a]; B. Lauke[a]; N. Perche[b]
[a] Institut für Polymerforschung Dresden e.V., Dresden, Germany [b] Centre de Recherches et d'Études d'Arcueil, Avenue prieur de la Cote d'Or, Arcueil Cedex, France

To cite this Article Schüller, T. , Beckert, W. , Lauke, B. and Perche, N.(1999) 'Analytical and Numerical Calculation of the Energy Release Rate for the Microbond-Test', The Journal of Adhesion, 70: 1, 33 — 56
To link to this Article: DOI: 10.1080/00218469908010486
URL: http://dx.doi.org/10.1080/00218469908010486

J. Adhesion, 1999, Vol. 70, pp. 33–56
Reprints available directly from the publisher
Photocopying permitted by license only

Analytical and Numerical Calculation of the Energy Release Rate for the Microbond-Test

T. SCHÜLLER[a,*], W. BECKERT[a], B. LAUKE[a] and N. PERCHE[b]

[a]*Institut für Polymerforschung Dresden e.V., Hohe Straße 6, 01069 Dresden, Germany;*
[b]*Centre de Recherches et d'Études d'Arcueil, Avenue prieur de la Cote d'Or, 94114 Arcueil Cedex, France*

(Received 15 June 1998; In final form 6 January 1999)

The energy release rate for interface crack propagation for the Microbond-Test specimen is calculated by using several stress analysis methods. For the corresponding finite element calculation an axisymmetrical model (elliptical droplet) and linear elastic material properties are used. The analytical approximations use several stress analysis methods to obtain the energy release rate.

The resulting energy release rate curves suggest that the debonding process can be described at least partially as a stable crack propagation along the interface. Some experiments confirm this prediction. The matrix droplet contribution to the energy release rate can be considerable. Because of the very complex stress fields in the droplet a simple analytical approximation cannot be given. The qualitative dependences on the material properties and on the geometry can be explained from the presented analysis. The remaining correction factor can be obtained from a numerical calculation.

Keywords: Microbond-Test; finite element analysis; adhesion; interface

INTRODUCTION

Adhesion between fibre and matrix in fibre-reinforced composite materials is expected to have an essential influence on strength and toughness of these composites. Micromechanical tests are often used

*Corresponding author. Tel.: (49-351) 4658-292, Fax: (49-351) 4658-284, e-mail: schuellr@argos.ipfdd.de

to evaluate the adhesion for a given fibre-matrix system and to test the influence of different surface treatments *via* data reduction of the load *versus* displacement curves.

One of these tests in the Microbond-(MB)-Test (developed by Miller *et al.* [1]) which is very similar to the Single-Fibre Pull-Out-(SFPO)-Test. It is preferably used by various experimentalists due to its relatively simple preparation. A small amount of the matrix material is deposited on a single fibre forming a droplet. After curing, the droplet is debonded by an axial displacement of the free fibre end relative to a microvise that shears away the droplet as shown in Figure 1. During

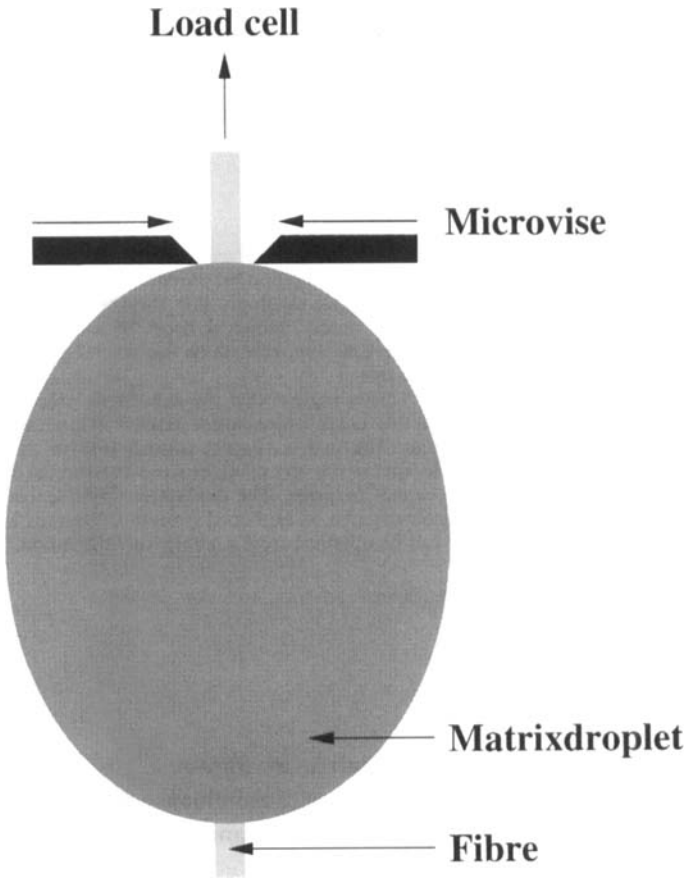

FIGURE 1 The Microbond-Test.

the failure process the fibre end is pulled at constant speed and the applied load is measured continuously. An example of commonly measured load *versus* displacement curves is depicted in Figure 2. The load increases with increasing displacement until a maximum load P_{max} is reached, then drops rapidly.

The conventional data reduction scheme assumes that the interface failure does not initiate until the point of maximum load is reached and that it progresses catastrophically after initiation. An interface parameter describing the adhesion quality is calculated from the maximum load, for instance an interfacial shear strength (commonly used) or a critical energy release rate for initiation of an interfacial debond [2].

Advanced experiments, especially providing the possibility of monitoring the fracture process, show that often a debonding process starts long before the maximum load is reached and progresses stably as a

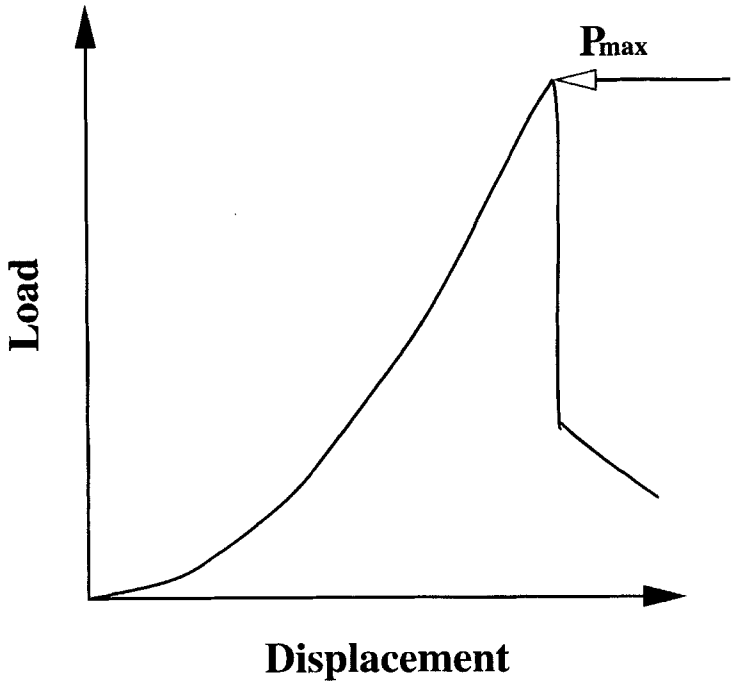

FIGURE 2 Example of load *versus* displacement curves.

propagating interface crack (SFPO-Test [3], MB-Test Fig. 3). Therefore, the assumptions for the commonly-used data reduction scheme mentioned above seem to be inappropriate.

A foregoing analysis of the SFPO-Test [4, 5] has shown that the debonding process (crack propagation) can be described by using fracture mechanics. The stable crack propagation is caused by an energy release rate that is nearly independent of the crack length. This independence of the crack length should result in a plateau range in the experimentally-observed load *versus* crack length curves. In reality, experimental curves show a nearly constant increase of the total load. This is due to the influence of a frictional shear stress. Reference [5] gives an empirical method to separate the frictional part of the total load resulting in an approximation for the "pure" plateau debonding force. The relationship between the approximated debonding force and the interface parameter (critical energy release rate, G_c) can be obtained from a simple analytical model. An essential point for this

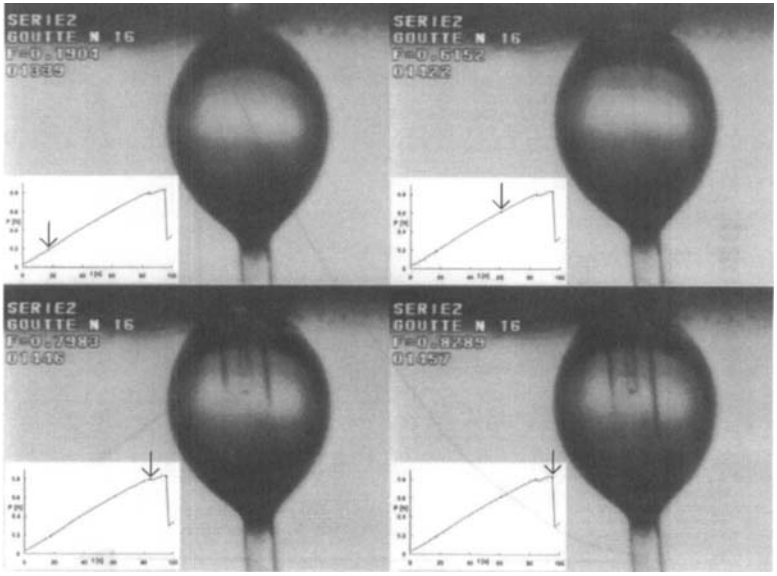

FIGURE 3 Four snapshots from a video-monitored MB-Test (glass-fibre-PE-system). The corresponding point in the load *versus* time curve is indicated (time $\propto$ displacement). Note that due to the magnifying effect of the droplet the crack length cannot be determined from the visible position of the crack tip.

method is that the large interfacial friction is mainly caused by surface roughness.

In our previous paper [6] we have carried out an analogous analytical and numerical approach to the MB-Test. The numerical model includes interfacial friction caused by surface roughness. Therefore, the simulated load *versus* displacement curves and load *versus* crack length curves are very similar to those that are observed in reality. An example is shown in Figure 4. The empirical method to separate the frictional contribution to the total load can be used here, too, as shown in Figure 4 (dashed lines). Therefore, the suggested data reduction scheme is the following:

1. Experimental measurement of load *versus* crack length curves.
2. Separation of the frictional part of the total load to obtain an approximate critical force for crack extension.
3. Calculation of the critical energy release rate (interface property) from the approximated critical force using an analytical model for the stress state in the specimen.

No. (1) seems very difficult; it requires advanced equipment. No. (3) needs a analytical model for the stress state in the specimen. For the SFPO-Test this problem is satisfactory solved because the main contribution to the energy release rate is provided by the free fibre [5]. By contrast, for the MB-specimen the matrix droplet can give a considerable contribution to the total energy release rate. This contribution depends on the droplet's geometry. In Ref. [6] we have given a

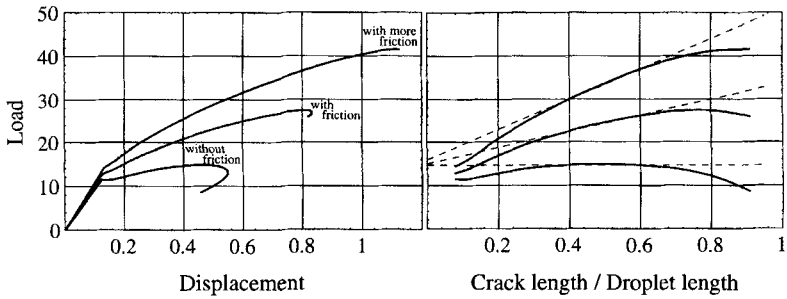

FIGURE 4 Examples of simulated load *versus* displacement and load *versus* crack length curves including frictional effects taken from Ref. [6].

rough analytical solution. Especially, the dependence of the droplet energy release rate on the droplet diameter cannot be confirmed by finite element calculations. Reference [2] also gives this dependence.

The aim of this paper is to develop a new analysis that describes correctly the dependence on the droplet's geometry. Starting from a numerical stress analysis, an analytical equation for the energy release rate is derived. The applicability and limits of the investigation are discussed at the end of the paper.

ENERGY RELEASE RATE

In a fracture mechanics approach the interface can be characterized by a critical energy release rate. It is the energy which is necessary to extend the crack. This interface property has to be measured by an experiment. Because it cannot be directly measured it must be calculated from other measured critical quantities, for instance critical forces, displacements or similar quantities. The energy release rate, G, of a given specimen containing a crack of length l_d is defined by the change of the total potential energy during an infinitesimal crack extension

$$G = \frac{1}{B}\frac{\partial(W_{\text{ext}} - U)}{\partial l_d} \tag{1}$$

where B denotes the width of the crack front. The influence of residual thermal stresses are discussed later and disregarded here. In this case, the energy release rate can be calculated from the change of the stored elastic strain energy, U, per newly formed crack area, Bdl_d, by (considering the case of constant external load, P)

$$G(l_d, P) = \frac{1}{B}\frac{\partial U}{\partial l_d}\bigg|_{P=\text{const.}} \tag{2}$$

The stored elastic strain energy can be derived from a stress analysis for a constant crack length using the integral of stresses, σ, multiplied

by strain, ε, over the volume of the whole specimen, V, by

$$U(l_d, P) = \frac{1}{2}\int_V \sigma(l_d, P)\varepsilon(l_d, P)\, dV \tag{3}$$

or using the integral of external load, P, multiplied by displacement, u, with respect to the surface, S, of the specimen by

$$U(l_d, P) = \frac{1}{2}\oint_S \vec{P} d\vec{u} \tag{4}$$

On the other hand, crack extension occurs at the crack tip. As a consequence, the energy release rate can be derived from the local fields at the crack tip. According to [7] the dominant stress singularity along the ligament can be written as

$$\sigma_{\theta\theta} + i\sigma_{\rho\theta}|_{\theta=0} = \frac{K\rho^{i\varepsilon}}{\sqrt{2\pi\rho}} \tag{5}$$

where ε denotes the bimaterial constant ($\varepsilon = 0$ for homogeneous material) and K the complex K-factor (see Fig. 5). Crack extension is considered here along the interface. The energy release rate is related

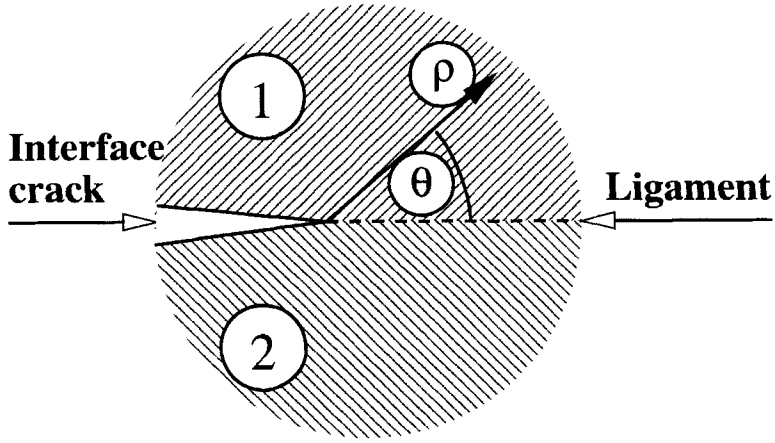

FIGURE 5 Near crack tip region along the interface.

to the crack tip fields by [8]

$$G(K(l_d, P)) = \frac{(1-\nu_1^2)E_2 + (1-\nu_2^2)E_1}{2\cosh^2(\pi\varepsilon)E_1E_2}|K|^2 \tag{6}$$

The K-factor can be obtained from a stress analysis. The bimaterial constant ε is given by

$$\varepsilon = \frac{1}{2\pi}\ln\left(\frac{(3-4\nu_1)(1+\nu_1)E_2 + (1+\nu_2)E_1}{(3-4\nu_2)(1+\nu_2)E_1 + (1+\nu_1)E_2}\right) \tag{7}$$

assuming a plane strain condition. This is a good approximation for the interface region of an axisymmetrical specimen, provided that the fibre is rigid compared with the droplet as shown in [9]. A numerical check of this condition is given in [10].

This provides three different methods to calculate the energy release rate from a stress analysis; all these methods are used for the numerical calculations. The analytical approximation uses only Eqs. (2) and (3). On the other hand, a critical energy release rate (interface property) can be calculated from experimentally-measured critical forces.

NUMERICAL CALCULATIONS – FINITE-ELEMENT-MODEL

The numerical stress analysis is carried out with the finite element method. The FE-mesh is built using 8-node elements (6-node singular elements at the crack tip) and linear-elastic material properties. Figure 6 shows the used FE-mesh for a certain crack length. The shape of the droplet is assumed to be elliptical. Very small details like the wetting cone are neglected. Instead of two shearing blades an axisymmetrical constraint is used as indicated in Figure 6. This allows the use of an axisymmetrical model. The specific modelling of this constraint influences the energy release rate only for very short crack lengths ($l_d \leq 0.2 \times$ droplet length [10]).

The mesh is highly refined towards the crack tip (radius of singular elements = $r_f/1000$) to obtain correctly the singular fields at the crack tip. Due to the regular mesh design for the fibre and for the inner part of the droplet the local meshing around the crack tip remains

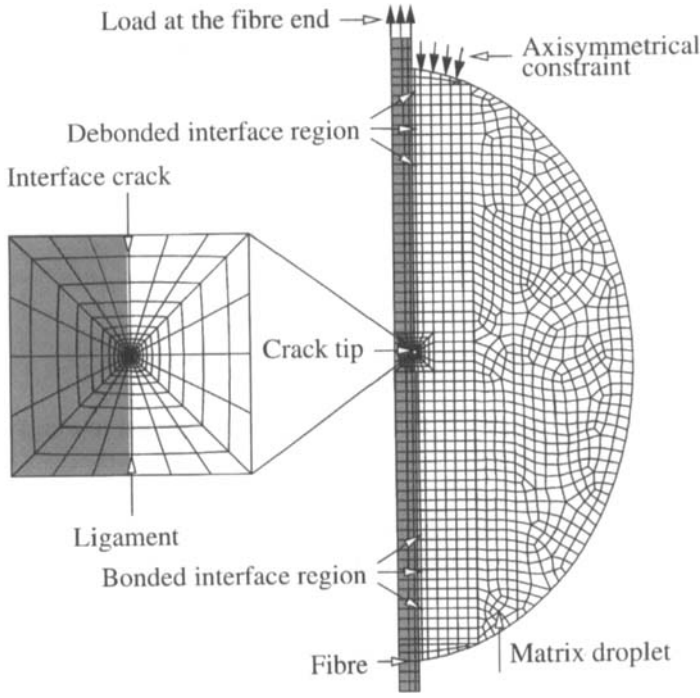

FIGURE 6 Finite element model for the MB-Test.

unchanged for the analysed sequence of crack-length steps. This minimizes the influence of the specific mesh.

The FE-analysis requires particular values for material properties and geometry. The following parameters were used: $E_f = 64\,\text{GPa}$, $\nu_f = 0.20$ (from a Schott-Glaswerke data sheet) and $r_f = 5\,\mu\text{m}$ for the fibre; $E_m = 3\,\text{GPa}$ and $\nu_m = 0.35$ for the matrix droplet (Epon828); $a = 75\,\mu\text{m}$ and $b = 60\,\mu\text{m}$ for the principal axes of the elliptical droplet. These values are representative for glass-epoxy systems. To check the validity of the analytical approximations some of these parameters are varied specifically. The calculations are performed using ANSYS 5.3 (PLANE 82 elements).

From the full FE-solution for a sequence of crack lengths, l_d, and a given load at the free fibre end, $P_0 = 80\,\text{mN}$, the elastic strain energy, U, the displacement of the free fibre end, u, and, using an extrapolation, the stress intensity factor, K, are calculated. Then interpolated

functions, $U(l_d, P)$, $u(l_d, P)$ and $K(l_d, P)$, are built using $U \propto P^2$, $u \propto P$ and $K \propto P$. The energy release rate is calculated from these functions by

$$G(l_d, P) = \frac{1}{2\pi r_f} \frac{\partial U(l_d, P)}{\partial l_d} \tag{8}$$

$$G(l_d, P) = \frac{1}{2\pi r_f} \frac{P}{2} \frac{\partial u(l_d, P)}{\partial l_d} \quad \text{or} \tag{9}$$

$$G(l_d, P) = \frac{(1 - \nu_f^2)E_m + (1 - \nu_m^2)E_f}{2\cosh^2(\pi\varepsilon)E_f E_m} |K(l_d, P)|^2 \tag{10}$$

The indices 1 and 2 in Eqs. (6) and (7) are now changed to f and m for fibre and matrix respectively.

By comparing the energy release rates calculated using these three different methods it is possible to check the consistency of the model. For the presented results these difference were less than 1.5%.

ANALYTICAL APPROXIMATION

For data reduction of experimental results an analytical equation is more useful. It is not practical to perform one numerical calculation for each experiment. The aim of this section is to derive an analytical equation for the energy release rate depending on the geometry and material properties of the MB-specimen and on the crack length.

The droplet shape is assumed to be elliptical as shown in Figure 7. So this analysis is different from those using a cylindrical droplet shape (for instance [2]). The energy release rate of the whole MB-specimen can be divided into fibre and droplet parts. From foregoing analysis [4, 2] it can be expected that the fibre part would give the main contribution. Consequently, first the fibre part is derived and then the droplet part is considered as a correction term. The influence of residual thermal stresses is treated separately in a special subsection.

Fibre Part

Figures 8, 9 and 10 show the stresses along the fibre surface for three different crack lengths. All stress fields are strongly inhomogeneous at

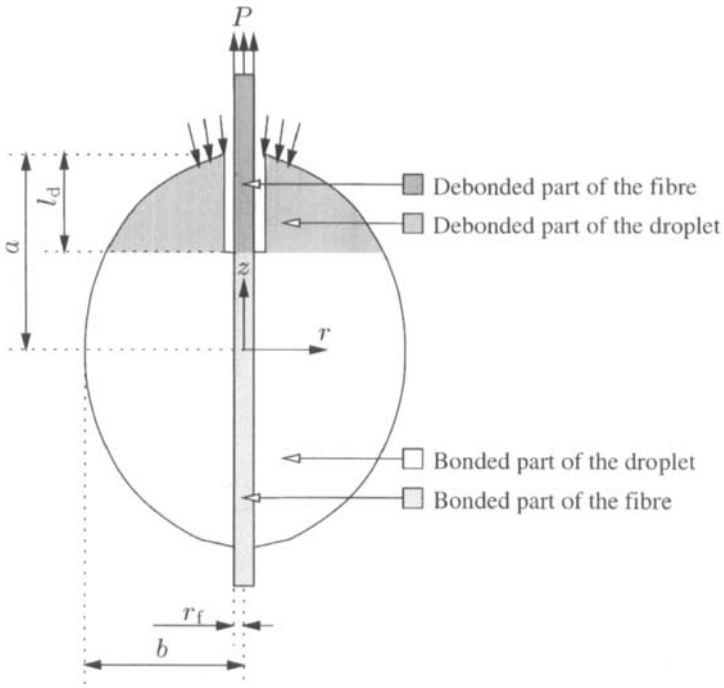

FIGURE 7 Elliptical model of the MB-Test (schematic).

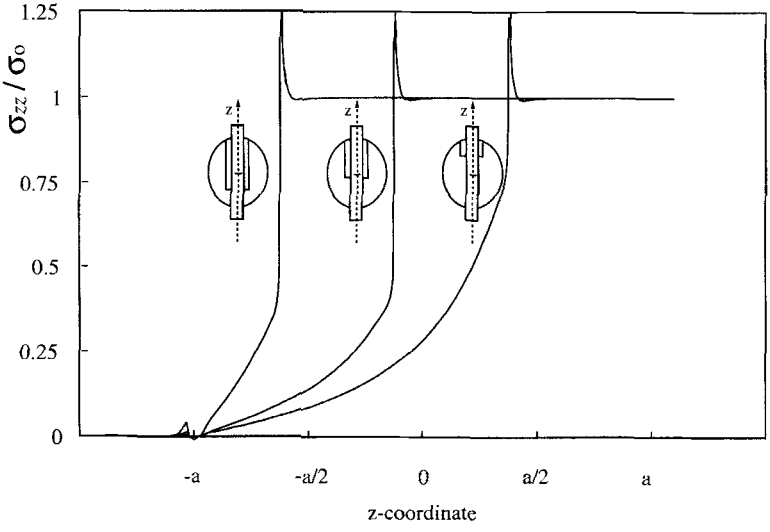

FIGURE 8 Normalized axial stress at the interface from the FE-analysis for three crack lengths 0.31, 0.56 and 0.81 × droplet length. The applied load is $P = 80\,\text{mN}$ ($\hat{=} \sigma_0 = 1\,\text{GPa}$).

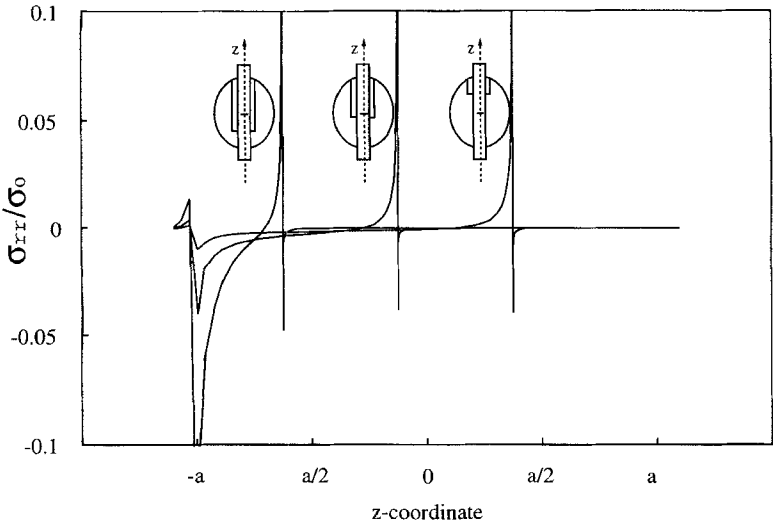

FIGURE 9 Normalized tensile stress at the interface from the FE-analysis for three crack lengths 0.31, 0.56 and 0.81 × droplet length. The applied load is $P = 80\,\text{mN}$ ($\hat{=}\,\sigma_0 = 1\,\text{GPa}$).

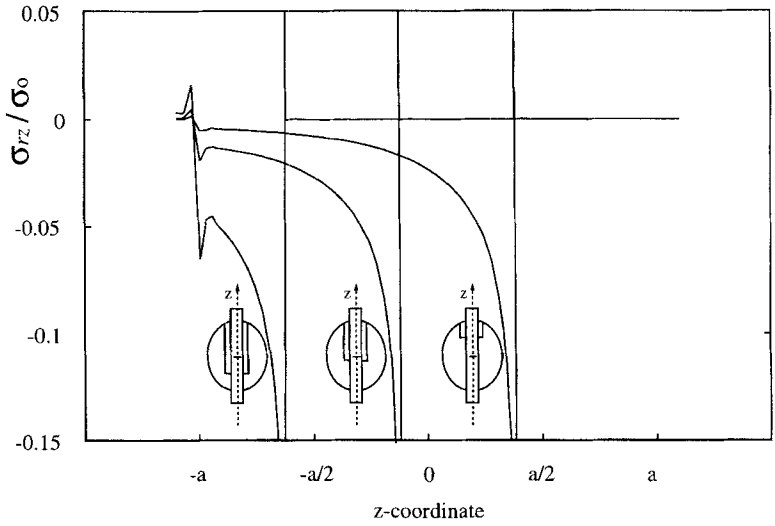

FIGURE 10 Normalized shear stress at the interface from the FE-analysis for three crack lengths 0.31, 0.56 and 0.81 × droplet length. The applied load is $P = 80\,\text{mN}$ ($\hat{=}\,\sigma_0 = 1\,\text{GPa}$).

the crack tip and at the fibre escape point. Nevertheless, the energy release rate contributions of these singularities are negligible because they are limited to a small area near the interface and they remain nearly unchanged (singularities at the fibre escape point) or move (singularities at the crack tip) during crack advance. Additionally, the $\sigma_{rr}^{(f)}$ and $\sigma_{rz}^{(f)}$ stress components are small compared with the $\sigma_{zz}^{(f)}$ component (note the different stress scales in Figs. 8, 9 and 10). The component $\sigma_{zz}^{(f)}$ is nearly homogeneous in the debonded part of the fibre

$$\sigma_{zz}^{(f)} = \frac{P}{\pi r_f^2} \tag{11}$$

$\sigma_{zz}^{(f)}$ drops rapidly in the bonded part. The fibre part of the energy release rate can be approximately calculated considering only the debonded part of the fibre. This part of the fibre extends when the crack propagates and gives the main contribution. According to this, the fibre part of the energy release rate can be estimated considering only the energy release rate of the free fibre end. The stored strain energy in the debonded part of the fibre is given by

$$U_f(l_d, P) = \frac{1}{2} \frac{(\sigma_{zz}^{(f)})^2}{E_f} \pi r_f^2 l_d \tag{12}$$

Using Eqs. (2), (11) and the new formed crack area, $B = 2\pi r_f dl_d$, results in

$$G_f(P) = \frac{P^2}{4\pi^2 r_f^3 E_f} \tag{13}$$

which is equivalent to the free fibre contribution derived by Outwater *et al.* [11] for the SFPO-Test.

Results for the part of the energy release rate from the FE-analysis normalized by Eq. (13) are shown in Figure 11 for different droplet sizes and different matrix stiffnesses. It can be seen that Eq. (13) is a good approximation for the fibre part.

Droplet Part

In a first attempt the droplet part of the energy release rate was obtained similarly to the estimation of the fibre part. The stress

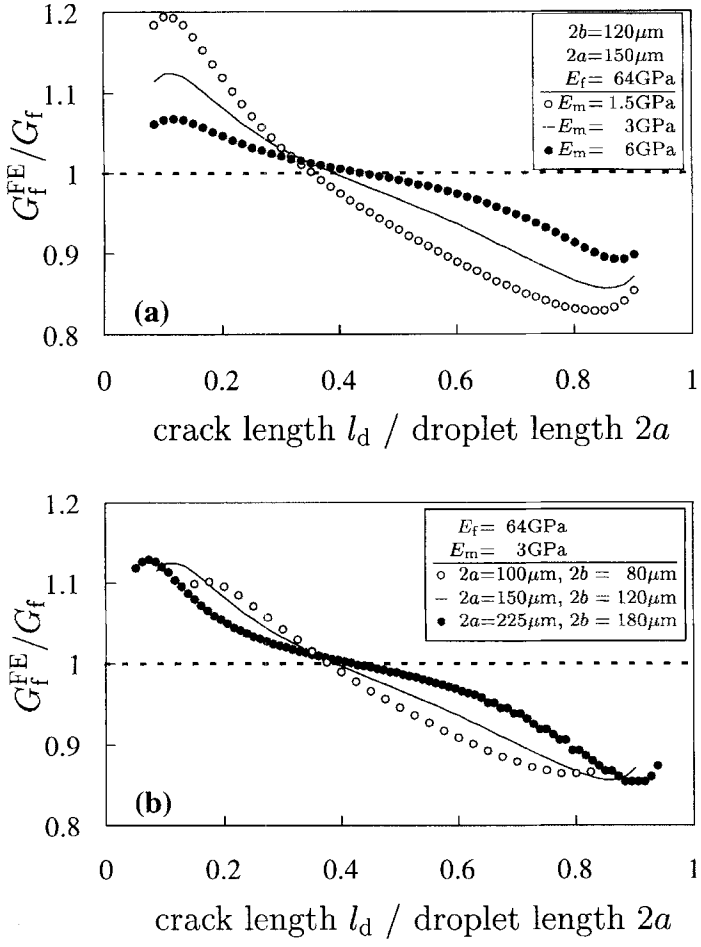

FIGURE 11 Normalized fibre part of energy release rate *versus* crack length from the FE-results for different droplet stiffnesses (a) and for different droplet sizes (b).

component $\sigma_{zz}^{(m)}$ is not homogeneous in the debonded part of the droplet, however. For a first approximation this stress component is assumed to be radially homogeneous. Then the dependence on z (or on the crack length, l_d, using $z = l_d - a$) can be obtained from the force balance as

$$\sigma_{zz}^{(m)}(l_d) = -\frac{1}{\pi}\frac{P}{(b(l_d))^2 - r_f^2} \tag{14}$$

where $b(l_d)$ is the droplet radius at the debonding position. Assuming $r_f^2 \ll (b(l_d))^2$ and replacing $b(l_d)$ using the elliptical shape of the droplet, $(b(l_d)/b)^2 + ((l_d - a)/a)^2 = 1$, results in

$$\sigma_{zz}^{(m)}(l_d) = -\frac{1}{\pi}\frac{P}{b^2}\frac{1}{1-(l_d/a-1)^2} \tag{15}$$

The droplet contribution to the energy release rate can be estimated taking into account only the debonded part using an argument similar to the above. The stored strain energy is derived from the assumed stress, $\sigma_{zz}^{(m)}(l_d)$, by

$$U_m(l_d, P) = \frac{1}{2}\int_0^{l_d} dl_d \int_0^{2\pi} d\varphi \int_{r_f}^{b(l_d)} dr \frac{(\sigma_{zz}^{(m)}(l_d))^2}{E_m} \tag{16}$$

in cylindrical co-ordinates (r, φ, l_d). There is no need to carry out the integral with respect to l_d because the energy release rate is the derivative of the strain energy with respect to l_d. Using again $r_f^2 \ll (b(l_d))^2$ results in

$$\begin{aligned} G_m^1(l_d, P) &= \frac{P^2}{4\pi^2 r_f^3 E_m}\frac{r_f^2}{b^2}\frac{1}{1-(l_d/a-1)^2} \\ &= G_f(P)\frac{E_f}{E_m}\frac{r_f^2}{b^2}\frac{1}{1-(l_d/a-1)^2} \end{aligned} \tag{17}$$

where the index 1 represents this simple approximation.

Results for the matrix part of the energy release rate obtained by the FE-analysis are shown in Figure 12 for different droplet sizes and different matrix stiffnesses. The curves show a symmetry relative to the center of the droplet. This symmetry appears also in Eq. (17) where it is caused by the elliptical geometry of the droplet. The influence of matrix stiffness on the estimated energy release rate, Eq. (17), is very well confirmed by the FE-analysis (Fig. 12a). Unfortunately, the dependence on the droplet diameter $2b$ is not confirmed (Figs. 12b and 12c). Changing the droplet diameter leaves the droplet part of the energy release rate nearly unchanged for large enough droplet diameters. Apparently, this part depends on the droplet length, $2a$, instead of the droplet diameter, $2b$.

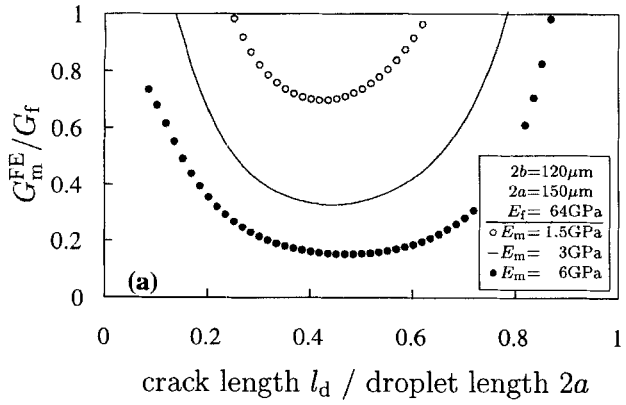

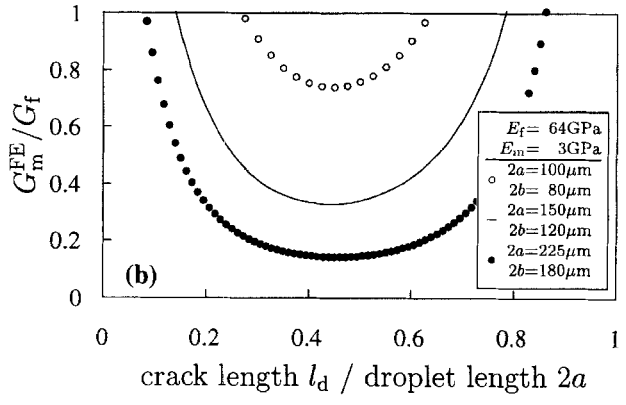

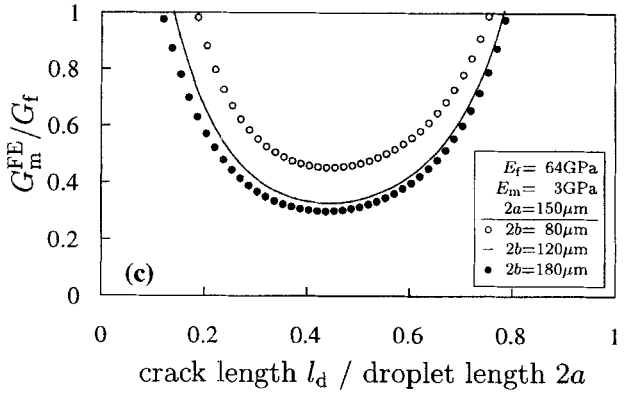

FIGURE 12 Normalized matrix part of energy release rate *versus* crack length from the FE-results for different droplet stiffnesses (a), different droplet sizes (b) and different droplet diameters (c).

This difference between the analytical solution and numerical results is not caused by the assumption of radially-homogeneous stress in the droplet. The analysis in [2] also gives this result. The reason for the differences is that the actual stress fields are not extended to the whole droplet but only to a region whose radius is associated with the fibre radius, because the microvise touches the droplet only in a small region near the fibre. Therefore, the stress fields as well as the energy release rate do not change if the droplet diameter is varied. Another consequence is that the symmetry of the energy release rate relative to the droplet centre mentioned above is not caused by the symmetrical droplet geometry.

It seems that the limit of a large droplet is already reached for commonly-used droplet geometry; the droplet border is far from the stress fields. A better estimation must include, in addition, the point loading at the top of the droplet as an essential factor. A simple approximation including all these items can be carried out as follows. The energy release rate of the droplet is estimated considering only the debonded part. For the stress analysis this part is considered to be a disc of thickness l_d and of large radius. This disc is loaded by two point forces acting against each other (see Fig. 13 Step 1). They represent the

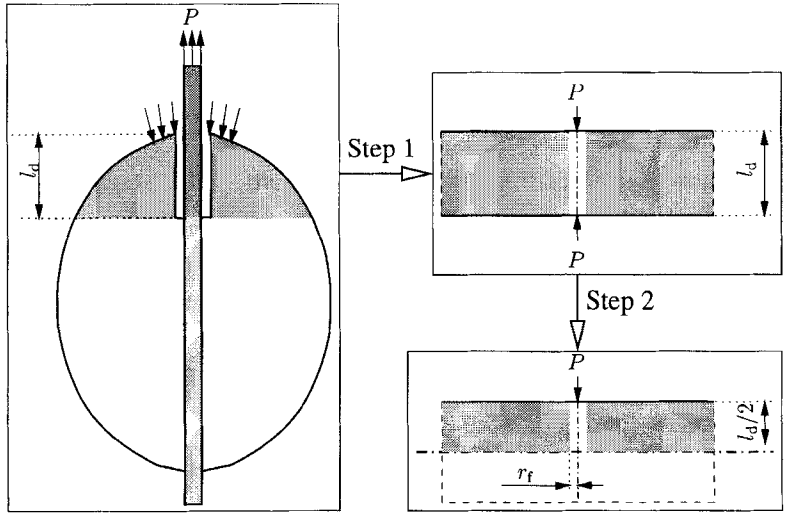

FIGURE 13 Disc model of the debonded part of the droplet (see text for a detailed explanation).

point loading caused by the microvise and the loading caused by the crack tip. To obtain the stress fields of such a disc a very simple estimation is used. It is based a on the stress fields of a filled half-space loaded at a point of its surface. Considering only loading vertical to the surface and only the $\sigma_{zz}^{(m)}$-component of the stress fields, the exact solution of this problem is [12]

$$\sigma_{zz}^{(m)}(r, \varphi, z) = -\frac{3z^3 P}{2\pi(r^2 + z^2)^{5/2}} \tag{18}$$

assuming a cylindrical coordinate system with the load P acting at the origin parallel to the z-axis. For the approximation of the stress fields in the disc this solution is cut off parallel to the surface of the half-space, obtaining a stress field for a disc of thickness $l_d/2$. Then this stress field is mirrored at the cutting plane obtaining an approximation for the stress field for the whole disc of thickness l_d (see Fig. 13 Step 2). The energy release rate is derived from this stress field by integrating over the whole disc, resulting in

$$\begin{aligned} G_m^D(l_d, P) &= \frac{P^2}{4\pi^2 r_f^3 E_m} \frac{9}{4} \frac{r_f^2}{a^2} \frac{1}{(l_d/a)^2} \\ &= G_f(P) \frac{9}{4} \frac{E_f}{E_m} \frac{r_f^2}{a^2} \frac{1}{(l_d/a)^2} \end{aligned} \tag{19}$$

The index D denotes this "disc-approximation". This rough estimation gives the predicted dependence on the droplet length. The essential point of this approximation is the point loading. It leads to the dependence above as shown in [10].

Total Energy Release Rate of the MB-specimen

The total energy release rate of the whole MB-specimen results from the sum of the fibre and the droplet part. With Eq. (13) for the fibre and Eqs. (17) and (19) these two relations are obtained

$$G^1(l_d, P) = G_f(P)\left(1 + \frac{E_f}{E_m} \frac{r_f^2}{b^2} \frac{1}{1 - (l_d/a - 1)^2}\right) \tag{20}$$

$$G^D(l_d, P) = G_f(P)\left(1 + \frac{9}{4}\frac{E_f}{E_m}\frac{r_f^2}{a^2}\frac{1}{(l_d/a)^2}\right) \tag{21}$$

The calculated energy release rates are compared with those from the FE-analysis for different droplet stiffnesses and droplet geometry in Figure 14. The energy release rate calculated in [2] is depicted, in addition. It can be seen that all of the derived analytical curves poorly fit the curves obtained from the FE-analysis. Nevertheless, these analytical considerations can be used to discuss some details of the debonding process.

Effect of Residual Thermal Stress

The preparation of the MB-specimen induces residual stresses due to thermal and/or resin-curing shrinkage. The following considerations are restricted to thermal effects; however, curing shrinkage effects would be similar.

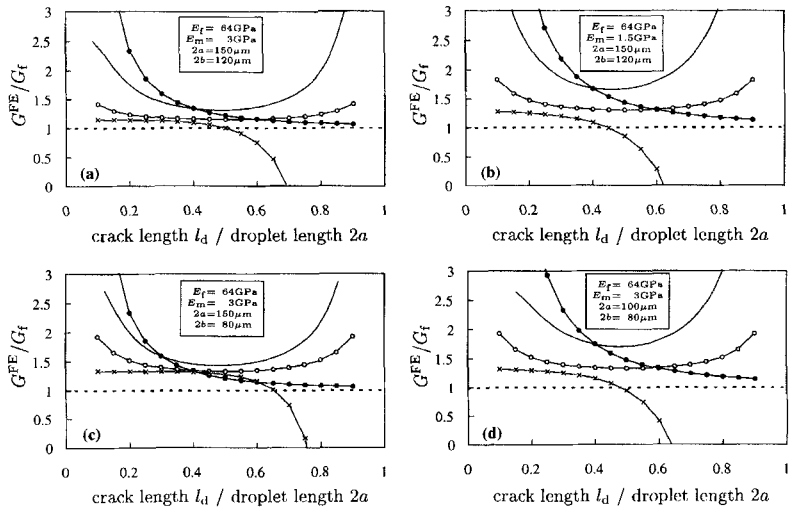

FIGURE 14 Normalized energy release rate of the MB-specimen *versus* crack length obtained from the FE-analysis (−), from Eq. (20) (○), from Eq. (21) (•) and from Ref. [2] (×). The energy release rates are calculated using different matrix stiffnesses (a, b) and different droplet geometry (c, d).

The contribution of residual thermal stresses to the total energy release rate have been already discussed in previous papers [13, 2, 5]. Reference [5] gives a correction term

$$G_f^{\text{therm}} = \frac{(\alpha_f - \alpha_m)\Delta T P}{2\pi r_f} \tag{22}$$

that describes the fibre contribution. This correction can also be used for the MB-Test. Figure 15 shows results for the energy release rate *versus* crack length obtained from a FE-calculation. In Figure 15a the total energy release rate is normalized using the energy release rate of the free fibre (Eq. (13)) while in Figure 15b the contribution of thermal stresses is subtracted first (by using Eq. (22)). It can be clearly seen that the effect of residual thermal stresses can be described by an additional correction term.

DISCUSSION

The stress state in the MB-specimen is very complicated. The matrix droplet can provide a considerable contribution to the energy release rate. Only for a crack extension in the middle part of the droplet ($0.4 < l_d/2a < 0.6$) and for a small contribution of the matrix droplet ($G_m/G_f < 0.5$) the analytical approximations give satisfactory results (see Fig. 14 and Tab. I). Now some basic problems are discussed in detail.

One problem is caused by the point loading from the microvise edges. The FE-analysis and all our analytical approximations result in energy release rate curves that drop sharply for shorter crack lengths ($l_d \ll a$). This means that the crack extension is expected to be stable in this range. Another consequence is that the limit for $l_d \to 0$ cannot be obtained as for the analysis in [2]. From the FE-analysis it seems that the exact behavior of the energy release rate for a very short crack length (or crack initiation) strongly depends on the conditions at the fibre entry point, such as the wetting cone, the exact position of the microvise edges, *etc.* [10]. In experiments two shearing blades are commonly used which produce large deformations at the top of the droplet. Including all these details in an analytical or numerical model seems unreasonable. Therefore, an energy release rate for the initiation of an interfacial debond should not be used.

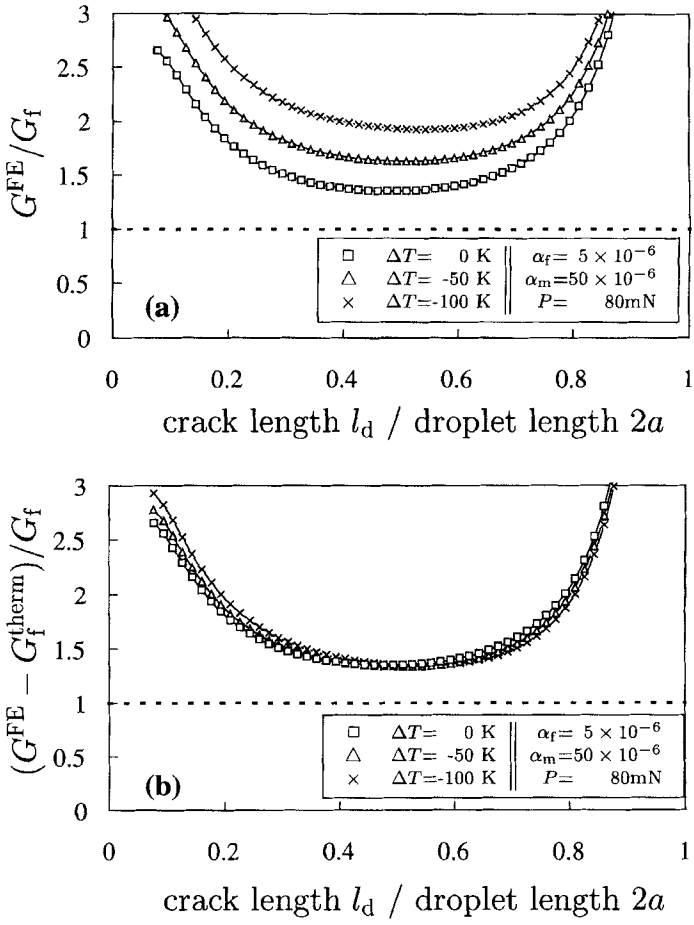

FIGURE 15 Normalized energy release rate of the MB-specimen *versus* crack length obtained from the FE-analysis including thermal stress.

Unfortunately, no wide "plateau range" (compared with the results for the SFPO-Test [4]) is found for the MB-Test. Only for crack extension in the inner part of the droplet not the energy release rate does change much (see Fig. 14). This range of stable crack propagation should be used for the determination of an interface parameter, for instance, the critical energy release rate. As seen in Figure 3 no plateau is observed in the experimental load *versus* displacement curves even though a propagating interface crack is observed. This is due to frictional effects as

TABLE I Qualitative comparison of the energy release rate obtained in the presented paper and taken from the literature

Energy release rate obtained from	*Range of the crack propagation*			*pattern in Figure* 14
	$l_d \to 0$	$l_d \approx a$	$l_d \to 2a$	
FE-calculation	Strongly increases	Has a wide minimum $G^{FE} - G_f \propto (r_f/a)^2$	Strongly increases	–
Our simple approximation	Strongly increases	Has a wide minimum $G^{1} - G_f \propto (r_f/b)^2$	Strongly increases	○
Our "disc" approximation	Strongly increases	Slightly decreases $G^{D} - G_f \propto (r_f/a)^2$	Slightly decreases	•
Ref. [2]	Becomes constant $G^{[2]} - G_f \propto (r_f/b)^2$	Slightly decreases	Strongly decreases	×

mentioned in the Introduction. The also-mentioned data reduction scheme (separation of the frictional contribution to the total load) requires load *versus* crack length curves. However, as can be seen in Figure 3 it seems to be promising to obtain crack length data. The simultaneous measurement of the crack length during the MB-experiment is very complicated. Even so, from the experiences with the SFPO-Test ([3 – 5]) we think it is worth while to improve the experiment in this regard.

A relationship between the (experimentally obtained) critical force for crack propagation and the critical energy release rate (interface parameter) that gives quantitatively satisfactory results for a wide range of material properties, and of geometry, cannot be given only from the presented analytical models. Nevertheless, the fundamental dependences on the material properties and on the geometry can be explained. Therefore, we suggest the following equation for data reduction

$$G_c = \frac{P_c^2}{4\pi^2 r_f^3 E_f}\left(1 + F \times \frac{E_f}{E_m}\frac{r_f^2}{a^2}\right) + \frac{(\alpha_f - \alpha_m)\Delta T P_c}{2\pi r_f} \qquad (23)$$

where F denotes a correction factor and P_c is the approximated critical force. Our "disc"-model results in $F = 9/4$. However, F can be obtained from a FE-calculation, too. The presented numerical results (Fig. 14) suggest a larger value, $F \approx 3.2$. Even so, all the given considerations will be valid only if the matrix droplet gives a small contribution to the total energy release rate of the specimen ($G_m < 0.4 G_f$). Nevertheless, this assumption is not a heavy restriction.

The finite element model is always used as a reference. In fact, it gives the best results for a specific set of parameters because it does not need additional assumptions. Nevertheless, it is based on linear elastic material properties and linear elastic theory. Therefore, it includes only a part of reality. Even so, the results show that from this point of view the experimental data can be qualitatively understood very well and also quantitatively interpreted.

Acknowledgements

Many thanks to Prof. U. Bahr, Technische Universität Dresden, for discussions and helpful hints. This work is supported by the Deutsche Forschungsgemeinschaft (project La818/3-2).

NOTATION

r_f	Fibre radius
$2a$	Droplet length
$2b$	Droplet diameter
l_d	Debonding crack length
E_f	Elastic modulus of the fibre
E_m	Elastic modulus of the matrix
α_f	Coefficient of thermal expansion of the fibre
α_m	Coefficient of thermal expansion of the matrix
ν_f	Poisson's ratio of the fibre
ν_m	Poisson's ratio of the matrix
ΔT	Cooling temperature difference
P	Load at the fibre end
u	Displacement of the fibre end
U	Strain energy
W_{ext}	Work done by external load
G	Energy release rate
K	Complex stress intensity factor
ε	Bimaterial constant

References

[1] Miller, B., Muri, P. and Rebenfeld, L., *Compos. Sci. Technol.* **28**, 17 (1987).
[2] Scheer, R. J. and Nairn, J. A., *Adhesion* **53**, 45 (1995).
[3] Hampe, A., Kalinka, G., Meretz, S. and Schulz, E., *Composites* **26**, 40 (1995).
[4] Beckert, W. and Lauke, B., *Computational Materials Science* **5**, 1 (1996).
[5] Beckert, W. and Lauke, B., *Composites Science and Technology* **57**, 1689 (1997).
[6] Schüller, T., Bahr, U., Beckert, W. and Lauke, B., *Composites Part A* **29A**, 1083 (1998).
[7] Rice, J. R., *Applied Mechanics* **55**, 98 (1988).
[8] Hutchinson, J. W. and Suo, Z., *Advances in Applied Mechanics* **29**, 63 (1992).
[9] Atkinson, C., Avila, J., Betz, E. and Smelser, R. E., *J. Mech. Phys. Solids* **30**, 97 (1982).
[10] Schüller, T., *Bruchmechanische Modellierung der Mixed-Mode-Belastung bei der Ausbreitung von Faser-Matrix-Grenzflächenrissen unter Berücksichtigung der nichtlinearen Reibungseffekte*, Master's thesis, Technische Universität Dresden, D-01069 Dresden, Germany (1997), in German.
[11] Outwater, J. D. and Murphy, M. C., *Modern Plastics* **47**, 160 (1970).
[12] Landau, L. D. and Lifschitz, E. M., *Lehrbuch der theoretische Physik, Bd. 7: Elastizitätstheorie* (Akademie-Verlag, Berlin, 1965), in German.
[13] Hutchinson, J. W. and Jensen, H. M., *Mechanics of Materials* **9**, 139 (1990).